molecules

MDPI

Article

Heterogeneous Photocatalysis as a Potent Tool for Organic Synthesis: Cross-Dehydrogenative C–C Coupling of *N*-Heterocycles with Ethers Employing TiO_2/*N*-Hydroxyphthalimide System under Visible Light

Elena R. Lopat'eva, Igor B. Krylov *, Oleg O. Segida, Valentina M. Merkulova, Alexey I. Ilovaisky and Alexander O. Terent'ev *

N. D. Zelinsky Institute of Organic Chemistry, Russian Academy of Sciences, 47 Leninsky Prospekt, 119991 Moscow, Russia

* Correspondence: krylovigor@yandex.ru (I.B.K.); alterex@yandex.ru (A.O.T.)

Abstract: Despite the obvious advantages of heterogeneous photocatalysts (availability, stability, recyclability, the ease of separation from products and safety) their application in organic synthesis faces serious challenges: generally low efficiency and selectivity compared to homogeneous photocatalytic systems. The development of strategies for improving the catalytic properties of semiconductor materials is the key to their introduction into organic synthesis. In the present work, a hybrid photocatalytic system involving both heterogeneous catalyst (TiO_2) and homogeneous organocatalyst (*N*-hydroxyphthalimide, NHPI) was proposed for the cross-dehydrogenative C–C coupling of electron-deficient *N*-heterocycles with ethers employing *t*-BuOOH as the terminal oxidant. It should be noted that each of the catalysts is completely ineffective when used separately under visible light in this transformation. The occurrence of visible light absorption upon the interaction of NHPI with the TiO_2 surface and the generation of reactive phthalimide-*N*-oxyl (PINO) radicals upon irradiation with visible light are considered to be the main factors determining the high catalytic efficiency. The proposed method is suitable for the coupling of π-deficient pyridine, quinoline, pyrazine, and quinoxaline heteroarenes with various non-activated ethers.

Keywords: Minisci reaction; heterogeneous photocatalysis; *N*-hydroxyphthalimide; titanium dioxide; green chemistry; visible light photocatalysis

Citation: Lopat'eva, E.R.; Krylov, I.B.; Segida, O.O.; Merkulova, V.M.; Ilovaisky, A.I.; Terent'ev, A.O. Heterogeneous Photocatalysis as a Potent Tool for Organic Synthesis: Cross-Dehydrogenative C–C Coupling of *N*-Heterocycles with Ethers Employing TiO_2/*N*-Hydroxyphthalimide System under Visible Light. *Molecules* **2023**, *28*, 934. https://doi.org/10.3390/molecules28030934

Academic Editors: Alexey M. Starosotnikov, Maxim A. Bastrakov and Igor L. Dalinger

Received: 25 December 2022
Revised: 11 January 2023
Accepted: 13 January 2023
Published: 17 January 2023

1. Introduction

Heterogeneous photocatalysis in organic synthesis is a young and fast-growing area [1–5]. The semiconductor materials used in photocatalysis are inexpensive and widely available; their advantages include the ease of separation from organic products, stability and recyclability [1,5]. However, the development of this area is still hindered by several formidable obstacles, such as low catalytic efficiency due to the low degree of charge separation in photoexcited states and the fast recombination of electron–hole pairs [6,7], low visible light absorption and low selectivity due to the strong oxidation power of photogenerated valence-band (VB) holes in popular semiconductors (TiO_2, ZnO, Bi_2O_3, WO_3, etc.) [1,8]. This situation is reflected in the comparatively low number of synthetic methods in fine organic synthesis based on heterogeneous photocatalytic systems compared to the mainstream applications of heterogeneous photocatalysis: oxidative destruction of pollutants [9–11], hydrogen generation [12,13], CO_2 reduction [14–16] and water splitting [17].

Currently, the scope of synthetic transformations enabled by heterogeneous photocatalysis is much less diverse compared to the scope of homogeneous photoredox-catalyzed reactions. Heterogeneous catalysis is mainly used in comparatively simple reactions; for example, alkylarene benzylic oxidation [18–20], the oxidation of benzylamines [4,5,21,22],

alcohols [4,5] and sulfides [4,23], oxidative esterification [4], nitro-group reduction [4], thiolene reaction [24], alkene amination with aqueous ammonia [25] and the decarboxylation of carboxylic acids [26–28]. Cross-coupling reactions are much less developed and usually demand transition metal co-catalysts, such as palladium or nickel complexes [29–33].

UV irradiation, which is used frequently for the excitation of heterogeneous photocatalysts, is inconvenient due to safety issues, the comparatively high cost of UV light sources, incompatibility with common laboratory glassware (UV-transparent quartz is necessary) and possible side reactions due to the high energy of the light. The modification of heterogeneous photocatalysts, such as TiO_2, in order to shift their photoactivity spectrum from UV to visible light [10,34–37] is the key task for expanding the scope of their applications in organic synthesis, increasing selectivity and making the of use cheap and available light sources for catalyst activation possible. At present, the following modification approaches have been proposed: the immobilization of dyes (organic compounds or metal complexes) on the photocatalyst surface [34,38–41], doping with metal ions or non-metal elements [42,43], semiconductor coupling [7,44–49] and modification with organic molecules bearing hydroxyl or carboxyl groups [34,50–56], which demonstrate the occurrence of visible light absorption when adsorbed on the surface of a semiconductor.

NHPI/TiO_2 is one of the efficient catalytic systems activated by visible light based on industrially available substances (Scheme 1). The interaction of NHPI with the TiO_2 surface leads to the occurrence of visible light absorption, resulting in the photogeneration of phthalimide-*N*-oxyl radicals (PINO) [20,22]. In our previous work [20], we demonstrated that the NHPI/TiO_2 system could be successfully applied to the aerobic oxidation of alkylarenes under visible light irradiation (Scheme 1A). The conceptual novelty of this system arises from the conjunction of heterogeneous photocatalysis with homogeneous radical chain organocatalysis. A distinguishing feature of this system is the migration of PINO into the volume of solution, where the PINO/NHPI catalyzed radical chain process, once initiated on the TiO_2 surface, produces the target product without the need for additional light absorption [20]. Thus, the energy efficiency of photocatalysis is fundamentally improved by combining heterogeneous photocatalysis with homogeneous organocatalysis. In the presence of additional organocatalyst (2,2,6,6-Tetramethylpiperidin-1-yl)oxyl (TEMPO) the effective oxidative homocoupling of benzylamines [22] was achieved previously (Scheme 1B).

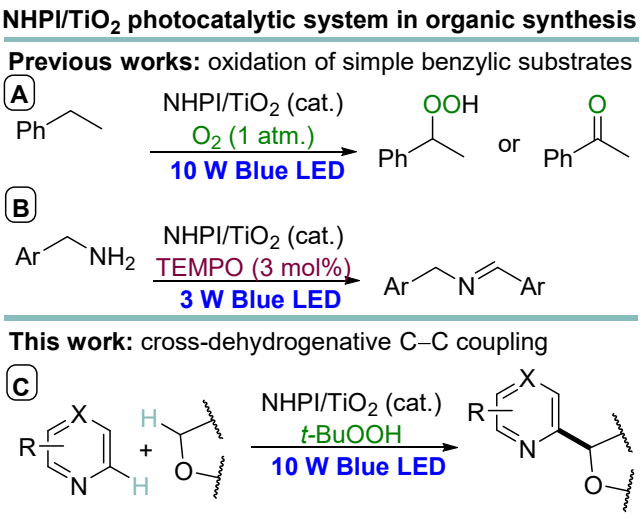

Scheme 1. Applications of NHPI/TiO_2 photocatalytic system in organic synthesis: CH-oxygenation (**A**) [20], oxidative homocoupling of benzylamines (**B**) [22], and Minisi-type corss-dehydrogenative C–C coupling reported in the present work (**C**).

In the present study, we demonstrate the successful application of the NHPI/TiO_2 system to a more challenging cross-dehydrogenative C–C coupling process (Scheme 1C).

In this case, previously reported CH-oxygenation processes [20] should be suppressed, which is a difficult task. In addition, the process of C–O coupling between NHPI-derived PINO radicals and CH-reagents [57–59] must be avoided. The oxidative coupling of ethers with π-deficient *N*-heteroaromatic compounds (a Minisci-type reaction) was chosen as a model reaction due to the practical importance for the functionalization of *N*-containing heterocycles with C–C bond formation. Minisci-type reactions [60–68] are based on the addition of nucleophilic C-centered radicals to electron-deficient arenes and represent one of the most important methods for the functionalization of such arenes, along with the nucleophilic aromatic substitution of hydrogen [69–71], and functionalization via transition-metal-catalyzed C(sp^2)–H bond activation [72–76]. The products of the Minisci reaction are of great value for medicinal chemistry [61,64]. Thus, the development of new, milder, more efficient methods tolerant to a large number of functional groups based on Minisci chemistry remains a hot research topic.

To date, many photochemical protocols have been developed for the Minisci reaction, both with the use of metal complex photocatalysts [60,77–80] and organic photocatalysts [81–83]. In some specific cases, the Minisci reaction proceeds without a photocatalyst [84–87]. At the same time, examples of the application of heterogeneous photocatalysis for the Minisci reaction that are attractive from the practical point of view remain rare [88–91]. In this work, we demonstrate the use of the developed hetero-/homogeneous NHPI/TiO_2 photocatalytic system for the Minisci reaction between π-deficient heteroarenes (pyridines, quinolines, isoquinolines, pyrazines, and quinoxaline) and non-activated ethers.

2. Results and Discussion

2.1. Optimization of Photocatalytic System Composition

Based on our previous work [20], TiO_2 with high specific surface area (anatase nanopowder, Hombikat UV100) and industrially available *N*-hydroxyphthalimide were chosen as the components of the photochemical system. Blue LEDs (455 nm) with an input power of 10 W were used as light sources. In the first step, we optimized the conditions of the photochemical cross-dehydrogenative Minisci reaction between 4-methylquinoline **1a** and tetrahydrofuran **2a** (Table 1). *Tert*-butyl hydroperoxide (TBHP) was used as an inexpensive, easily available and metal-free oxidant.

The starting conditions (10 mg of TiO_2, 20 mol.% of NHPI, 4 mmol of TBHP, 5 h, run 1) yielded 45% of the product **3aa**. The absence of either TiO_2 or NHPI resulted in the zero conversion of **1a** (runs 2, 3), proving that both components of the catalytic system are essential. Without *t*-BuOOH, the reaction proceeded with low efficiency: only trace amounts of the product were formed (run 4). As a rule, the addition of a strong Brønsted acid, such as HCl [85] or TFA [77,79,82,84,86], increases the efficiency of the Minisci reaction. Acids protonate π-deficient *N*-containing heterocycles, making them more susceptible to attack by nucleophilic C-centered radicals [67]. However, in our case, the addition of trifluoroacetic acid (TFA, run 5) had no significant effect on the yield and conversion. The addition of 0.5 mL of water resulted in a drop in **3aa** yield (run 6). Water breaks down the stable suspension of TiO_2 in THF, causing the catalyst particles to aggregate in the water droplets. Both an increase and a decrease in the amount of THF lead to a decrease in the yield of **3aa** (runs 7, 8). The dilution of the reaction mixture with such co-solvents as hexafluoroisopropanol (HFIP, run 9) and acetonitrile (MeCN, run 10) slowed down the reaction, and dilution with dichloroethane (DCE, run 11) led to the complete suppression of the target process. It is known that hydrogen peroxide can be used as the oxidant for the photocatalytic Minisci reaction [85]. However, the change of the oxidant from TBHP to aqueous H_2O_2 led to a dramatic drop in the yield (run 12). The lower efficiency of H_2O_2 compared to TBHP can be explained by the fact that H_2O_2 can not only initiate free-radical reactions but can also be an inhibitor via the formation of HOO• radicals [92–94]. The use of other organic peroxides, such as meta-chloroperoxybenzoic acid (m-CPBA, run 13), cumene hydroperoxide (run 14) and dicumyl peroxide (run 15) led to low yields or did not provide the product at all. Dibenzoylperoxide (BzOOBz, run 16) showed a yield comparable

to TBHP, but the formation of a large amount of benzoic acid, which is poorly soluble in the system, complicates the isolation of the products and limits the scalability of the procedure. Therefore, TBHP was chosen as the optimal oxidant. The standard version of the Minisci reaction often uses inorganic persulfates as oxidants. In our system, the use of persulfates was less efficient than TBHP, and led to a significant drop in yield with increasing reaction time, presumably due to the overoxidation of the product (runs 17–20). An inert atmosphere did not increase the selectivity of the process (run 21), so we decided to carry out the reaction under air.

Table 1. Influence of photocatalytic system composition, irradiation power, and nature of oxidant on the conversion of 4-methylquinoline **1a** and yield of **3aa** in photocatalytic Minisci reaction.

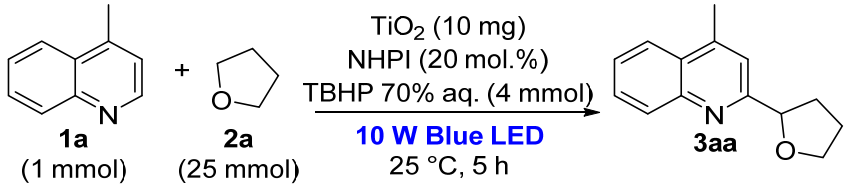

Run	Changes to the General Conditions	Conversion [a] 1a, %	Yield [a] 3aa, %
1	none	53	45
2	no TiO_2	0	0
3	no NHPI	0	0
4	no TBHP	6	4
5	TFA (1.5 mmol) added	52	45
6	H_2O (0.5 mL) added	23	9
7	THF (12.5 mmol)	38	36
8	THF (50 mmol)	32	27
9	HFIP (1 mL) added	18	16
10	MeCN (1 mL) added	17	16
11	DCE (1 mL) added	0	0
12	H_2O_2 34% aq. [b]	9	3
13	m-CPBA 75% aq. [b]	28	0
14	$PhCH(CH_3)_2OOH$ 80%	15	15
15	$PhCH(CH_3)_2OOPhCH(CH_3)_2$ 98% [b]	16	0
16	BzOOBz 75% aq. (1 mmol) [b]	59	44
17	$(NH_4)_2S_2O_8$ [b,c]	39	33
18	$Na_2S_2O_8$ [b,c]	36	22
19	$K_2S_2O_8$ [b,c]	44	39
20	$K_2S_2O_8$ [b,c], 16 h, Argon atmosphere	90	27
21	Argon atmosphere	44	39

[a] The conversion of **1a** and the yield of **3aa** were determined by ^1H NMR using $C_2H_2Cl_4$ as an internal standard. [b] instead of TBHP. [c] 1 mL of water was used as co-solvent to dissolve the persulfate.

In the next step, we optimized the NHPI/TiO_2/TBHP ratio and irradiation time to achieve the maximum yield of the coupling product **3aa** (Table 2).

Increasing the amount of TiO_2 increases the yield of **3aa** (runs 1–4). However, when switching from the TiO_2 loading of 20 mg to 40 mg, the efficiency increased only slightly. Therefore, the TiO_2 loading of 20 mg was chosen as the optimal amount. Similarly, large loadings of NHPI resulted in an increase in the **3aa** yield (runs 5–8), but the step from 20 to 40 mol.% of NHPI increased the yield of **3aa** slightly, and a slight drop in selectivity was observed. The optimum excess of THBP was 4 mmol per 1 mmol of **1a** (runs 9–11). The reaction proceeded with almost complete conversion in 8 h (run 15). It should be noted that visible-light-active heterogeneous photocatalyst g-C_3N_4 was ineffective for the model coupling reaction under the same conditions (run 16). The conditions of experiment 15 were chosen as optimal for further studies of the substrate scope for the developed method.

Table 2. Optimization of NHPI/TiO_2/TBHP ratio and reaction time for the synthesis of **3aa**.

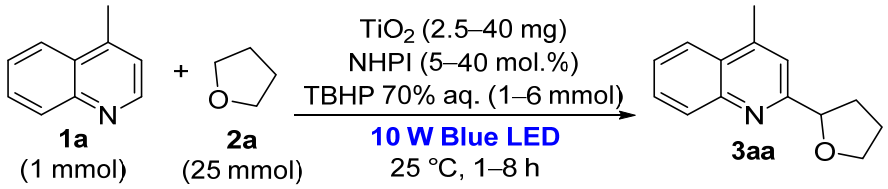

Run	TiO_2, mg	NHPI, mmol	TBHP, mmol	Time, h	Conversion [a] 1a, %	Yield [a] 3aa, %
1	2.5	0.1	2	5	5	5
2	5	0.1	2	5	12	11
3	20	0.1	2	5	44	40
4	40	0.1	2	5	55	46
5	10	0.05	2	5	0	0
6	10	0.1	2	5	39	36
7	10	0.2	2	5	44	39
8	10	0.4	2	5	52	41
9	10	0.1	1	5	31	27
10	10	0.1	4	5	49	42
11	10	0.1	6	5	38	38
12	10	0.1	2	1	5	4
13	10	0.1	2	2	20	15
14	10	0.1	2	5	34	28
15	20	0.2	4	8	96	89
16	- [b]	0.2	4	8	9	7

[a] The conversion of **1a** and the yield of **3aa** were determined by ^{1}H NMR using $C_2H_2Cl_4$ as an internal standard. [b] Bulk g-C_3N_4 (20 mg) was used instead of TiO_2 as heterogeneous photocatalyst.

2.2. Application of the Designed Photocatalytic NHPI/TiO_2 System to the Minisci Reaction

With the optimal conditions in hand (Table 2, run 15), we have synthesized a wide range of coupling products between *N*-heterocycles and ethers. The scope of ethers was explored first (Scheme 2). For substrates demonstrating lower conversions compared to **1a**, the reaction time increased in some cases up to 48 h (the reaction times and conversions are given in Scheme 2).

Among the tested ethers, we obtained the best result with THF: after 8 h of reaction, the almost complete conversion of 4-methylquinoline **1a** and a high yield of product **3aa** (89%) were observed. As a rule, the reaction proceeds more slowly and with lower selectivity for other ethers. In the reaction of 4-methylquinoline with 2-methyltetrahydrofuran **2b**, a mixture of products **3ab** (as a diastereomeric mixture, major) and **3ab'** (minor) was observed. The observed regioselectivity can be explained by the fact that although the hydrogen atom abstraction is most favored from the weakest tertiary CH-bond (position 2 of 2-methyltetrahydrofuran) [95], the resulting C-centered radical is more stable and sterically hindered than the secondary radical and reacts less efficiently with 4-methylquinoline. For 1,3-dioxolane **2c**, two isomeric products **3ac** and **3ac'** were formed, and the major product **3ac** corresponds to the breaking of the weakest C2-H bond in 1,3-dioxolane. With dioxane and tetrahydropyran, the reaction proceeded more slowly, but with a longer reaction time, its selectivity decreased simultaneously with an increase in conversion. With glyme, the dehydrogenative coupling product was not observed even after 24 h of reaction.

In the case of diethyl ether as a substrate, the reaction under the standard conditions was not effective due to the immiscibility of Et_2O and H_2O contained in TBHP (70% aq.), which led to the aggregation of TiO_2 particles in water droplets and the low conversion of **1a**. The solution to the problem was the use of anhydrous TBHP, prepared before the reaction (See experimental details for Scheme 2). The same problem limited the reaction time for the coupling of **1a** with Et_2O since the water generated during TBHP reduction accumulated in the reaction mixture and made the TiO_2 suspension unstable.

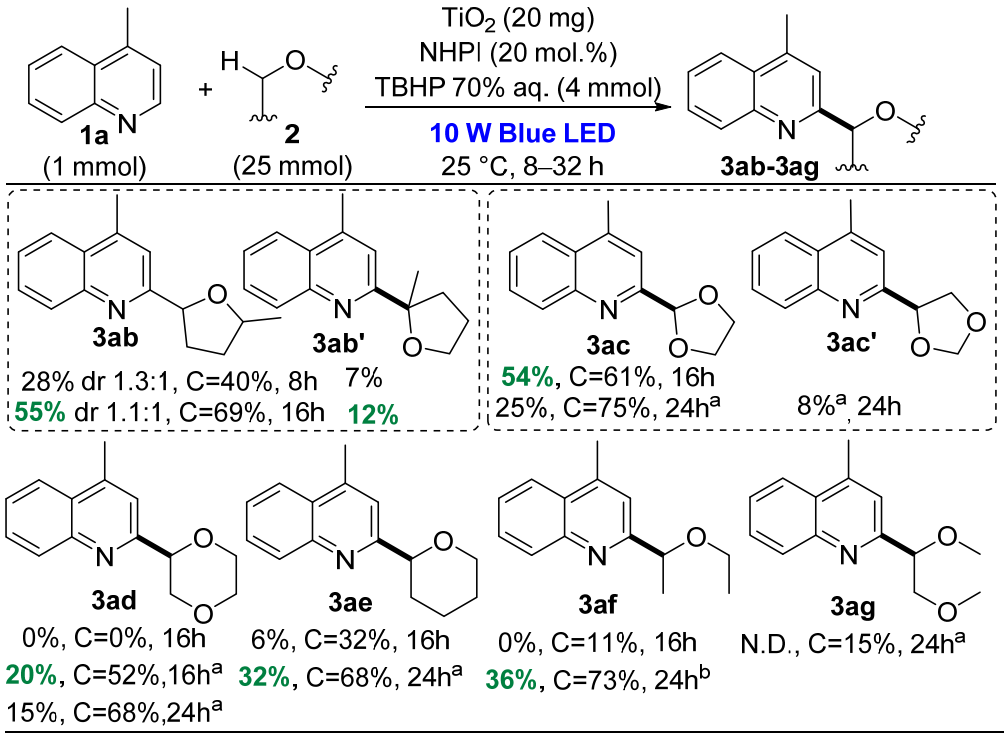

Scheme 2. Scope of ethers for the photocatalytic Minisci reaction with 4-methylquinoline **1a**.

In the next step, the scope of the electron-deficient *N*-heterocycles was tested (Scheme 3).

N-heterocycles with electron-donor groups reacted slower compared to substrates with electron-withdrawing groups, but at the same time, higher selectivity was observed (products **3ba**, **3ea** in comparison with **3ca**). The reaction is sensitive to steric hindrance: 2-chloro-5-bromoquinoline **2d** did not yield the target product of **3da**, presumably due to the presence of a bulky Br substituent near the 4th position of the quinoline. Our photochemical system is also applicable to quinoxalines and pyrazines. It is worth noting that the products of **3ga** and **3ha** have not been previously reported (See Supplementary Materials for additional information). In general, the reaction is inefficient for pyridines with no substituents or with electron-donor substituents (pyridine, picolines, lutidine), but good yields have been obtained for pyridines with electron-acceptor substituents, such as pyridine-3-carboxylic acid methyl ester (product **3ia**). 4-Methylquinoline-*N*-oxide reacted with the preservation of the *N*-oxide function (product **3ja**). Good yields have also been obtained in the reaction with isoquinoline (product **3ka**). In the reaction with imidazo [1,2-a]pyridine **2l**, it was only possible to isolate the product of deep oxidation with the destruction of the ring—**3la'**. It should also be noted that the addition of acid (TFA) afforded increased yields in some cases (products **3ba**, **3ca**, **3ea**, **3ga**, **3ha**,**3ja** and **3ka**).

It turned out that carrying out the reaction to complete the conversion of π-deficient arenes in the NHPI/TiO_2 photochemical system leads to a sharp drop in selectivity for target product **3**. We assumed that product **3** could undergo further oxidation under the reaction conditions. To find out what role the individual components of the system play in oxidation, we performed control experiments in which the pure reaction product **3aa** was placed under standard reaction conditions or irradiated in an inert atmosphere in the absence of NHPI or TBHP (Scheme 4).

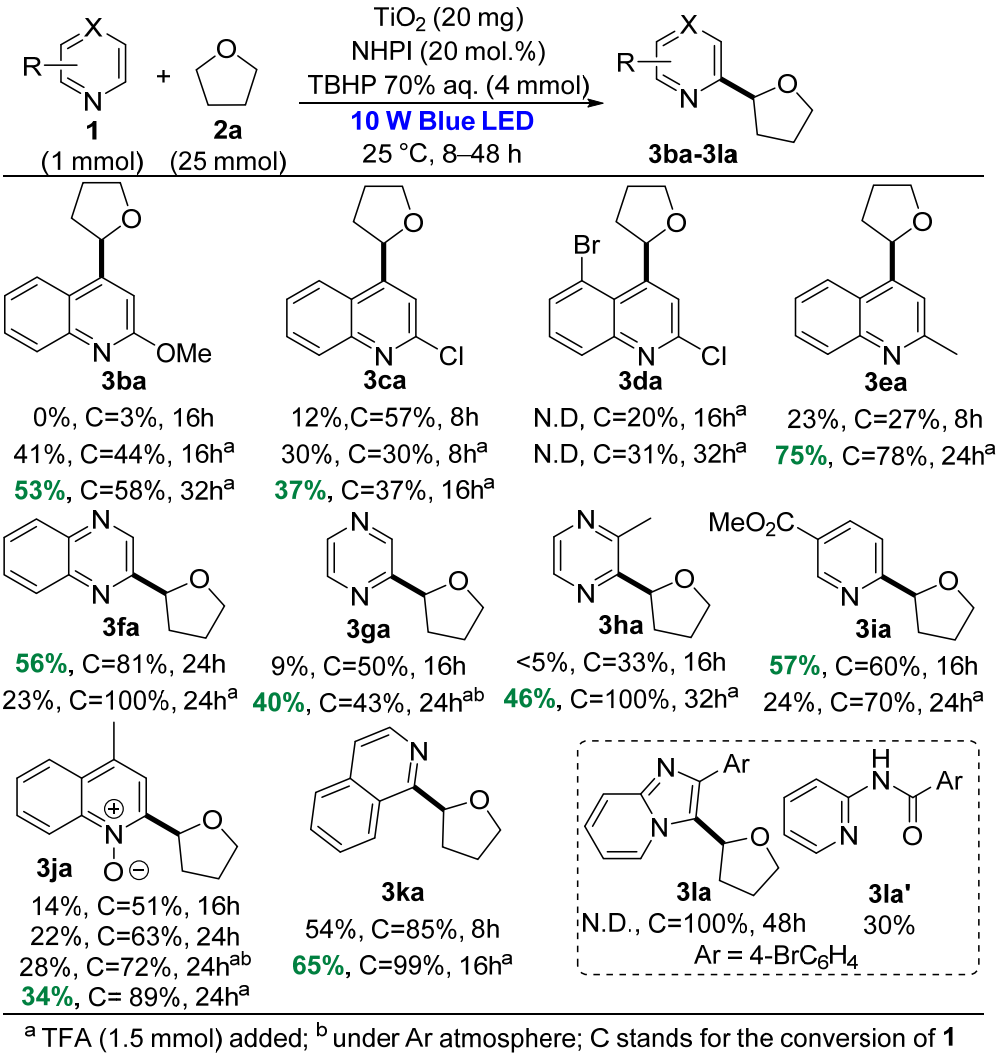

Scheme 3. Scope of π-deficient arenes for the photocatalytic Minisci reaction with tetrahydrofuran.

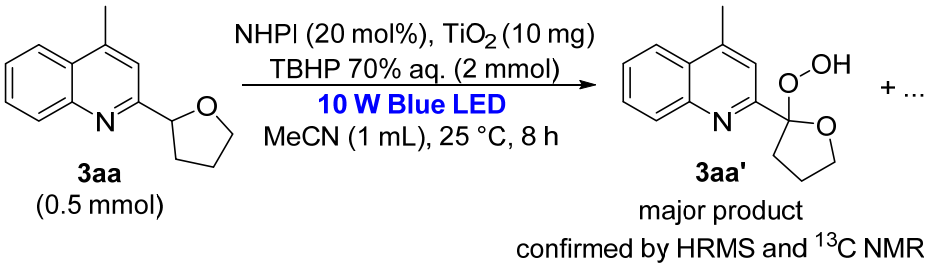

Conditions	Conversion of **3aa**, %
A. Air	86
B. Air, without TBHP	88
C. Ar	56
D. Ar, without NHPI	34

Scheme 4. Control experiments disclosing side processes of the photocatalytic Minisci reaction.

Under the standard conditions, an 86% conversion of **3aa** was observed in 8 h (Scheme 4, **A**). In the absence of TBHP under an air atmosphere, the product is also oxidized (88% conversion, Scheme 4, **B**), which suggests that a significant role in the decomposition of the product is played by air as an oxidant. The primary oxidation product was hydroperoxide **3aa'**, which was detected in a mixture of oxidation products by ^{13}C NMR

and was confirmed by HRMS (See Supplementary Materials). The ^{13}C signal with chemical shift typical for geminal alkoxyhydroperoxide fragment was observed [96]. However, carrying out the reaction under an argon atmosphere (Scheme 4, **C**) does not completely suppress the oxidation of product **3aa** since TBHP or residual amounts of oxygen can serve as oxidants. The lowest conversion of the product was observed when the reaction was carried out in an argon atmosphere without the addition of NHPI (Scheme 4, **D**), implying that NHPI-derived PINO radicals play an important role in **3aa** oxidation.

Based on the collected data, we proposed the following mechanism (Scheme 5). Upon irradiation with visible light, PINO radicals are generated from NHPI on the TiO_2 surface. Simultaneously, the *tert*-butyl hydroperoxide decomposes on the TiO_2 surface with the formation of *tert*-butoxyl radicals. *Tert*-butoxyl radicals can regenerate PINO by abstracting a hydrogen atom from the NHPI in solution [59]. *Tert*-butoxyl radicals can also generate *tert*-butylperoxy radicals from *t*-BuOOH [97,98]. Either *tert*-butoxy, *tert*-butylperoxy [99–101], or PINO radicals [59,95] can abstract a hydrogen atom from the α-CH bond in ether to form C-centered radical **A**. However, considering the fact that no cross-dehydrogenative coupling was observed without the addition of NHPI, the main role in H-atom abstraction is assumed to be played by the PINO radicals. Then, radical **A** undergoes addition to a heteroarene with the formation of the intermediate radical **B**, which is further subjected to HAT with the retrieval of aromaticity.

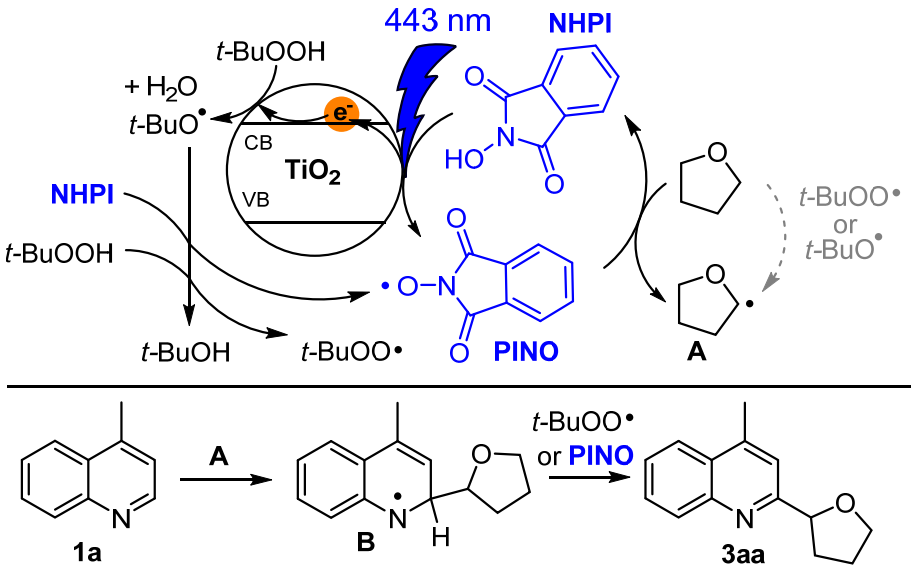

Scheme 5. Plausible mechanism of the photocatalytic Minisci reaction.

3. Materials and Methods

3.1. General

Room temperature (rt) stands for 23–25 °C.

Commercial TiO_2 Hombikat UV 100 (anatase, specific surface area, BET: 300 $m^2 \cdot g^{-1}$, primary crystal size according to Scherrer <10 nm) was used as is. *N*-hydroxyphthalimide (NHPI, 98%, Acros Organics), 4-methylquinoline (99%, Acros Organics), 2-methylquinoline (97%, Acros Organics), 2-chloroquinoline (99%, Acros Organics), isoquinoline (97%, Acros Organics), quinoxaline (99%, Acros Organics), pyrazine (99+%, Acros Organics), 2-methylpyrazine (99+%, Acros Organics), Methyl nicotinate (99%, Acros Organics), 2-methoxyquinoline, 5-bromo-2-chloroquinoline were used as is from commercial sources. 4-methylquinoline 1-oxide was synthesized according to the literature procedure [102], 2-(4-bromophenyl)imidazo [1,2-a]pyridine was synthesized according to the procedure in the literature [103]. Bulk g-C_3N_4 was prepared analogously to previously reported methods [104,105], and the urea was heated in a covered alumina crucible for 4 h at 550 °C (heating rate 5 °C·min−^{1}). MeCN was distilled over P_2O_5, and Ethers (THF, 2-Methyltetrahydrofuran, 1,3-dioxolane,

1,4-dioxane, tetrahydropyran and diethyl ether, dimethoxyethane, bis(2-methoxyethyl) ether) were distilled over $LiAlH_4$. The reaction mixtures were sonicated in an ultrasonic bath (HF-Frequency 35 kHz, ultrasonic nominal power 80 W) before the irradiation.

Experimental details for Table 1

General reaction conditions: 4-methylquinoline **1a** (1 mmol, 143.2 mg), TiO_2 (10 mg), NHPI (0.2 mmol, 32.6 mg), *t*-BuOOH (70% aq., 4 mmol, 515 mg), THF **2a** (25 mmol, 2 mL) and a magnetic stir bar (6 × 10 mm) were placed in a 50 mL round-bottom flask. The obtained mixture was sonicated for 5 min in an ultrasonic bath, then magnetically stirred (500 rpm) in a thermostated water bath at 25 °C (±1 °C) under irradiation of 10 W blue LED for 5 h under an air atmosphere (closed flask). Then, the solvent was rotary evaporated, and $C_2H_2Cl_4$ (40–60 mg, 0.4–0.61 mmol) was added as a standard for NMR yield determination. The reaction mixture was centrifuged, and the NMR spectrum was recorded.

Experimental details for Table 2

4-methylquinoline **1a** (1 mmol, 143.2 mg), TiO_2 Hombikat UV 100 (2.5–40 mg), NHPI (0.05–0.4 mmol, 8.2–65.2 mg), *t*-BuOOH 70% aq. (1–6 mmol, 129–772 mg) and THF **2a** (25 mmol, 2 mL) and a magnetic stir bar (6 × 10 mm) were placed in a 50 mL round-bottom flask. The obtained mixture was sonicated for 5 min in an ultrasonic bath, then magnetically stirred (500 rpm) in a thermostated water bath at 25 °C (±1 °C) under irradiation of 10 W blue LED for 1–16 h under an air atmosphere (closed flask). Then, the solvent was rotary evaporated, $C_2H_2Cl_4$ (40–60 mg, 0.4–0.61 mmol) was added as a standard for NMR yield determination. The reaction mixture was filtrated through a Celite layer, and the NMR spectrum was recorded.

Experimental details for Schemes 2 and 3

Heterocycle **1** (1 mmol), TiO_2 (20 mg), NHPI (0.2 mmol, 32.6 mg), *t*-BuOOH 70% aq. (4 mmol, 515 mg), CH-reagent **2** (25 mmol) and a magnetic stir bar (6 × 10 mm) were placed in a 50 mL round-bottom flask. The obtained mixture was sonicated for 5 min in an ultrasonic bath, then magnetically stirred (500 rpm) in a thermostated water bath at 25 °C (±1 °C) under irradiation of 10 W blue LED for 8 h under an air atmosphere (closed flask). If needed, another 4 mmol of the reaction *t*-BuOOH was added, and the reaction mixture was irradiated for another 8 h. At the end of the required time, the reaction mixture was poured into 20 mL of water and extracted with 3×15 mL of CH_2Cl_2. The combined organic extracts were washed with 2 × 20 mL of $NaHCO_3$ saturated solution. The extracts were dried over $MgSO_4$, and the solvent was evaporated in a vacuum membrane pump. The residue was purified using column chromatography to afford products **3aa**–**3ka**. For the reaction of **1a** with Et_2O, anhydrous *t*-BuOOH was prepared. *t*-BuOOH 70% aq. (12 mmol, 1545 mg) was extracted with CH_2Cl_2 (10 mL). The organic layer was dried over $MgSO_4$, and the solvent was rotary evaporated. The obtained anhydrous *t*-BuOOH was used instead of *t*-BuOOH 70% aq. For the longer reaction times, the new portion of anhydrous *t*-BuOOH (4 mmol, 360 mg) was added each 8 h.

Experimental details for Scheme 4

4-methyl-2-(tetrahydrofuran-2-yl)quinoline **3aa** (0.5 mmol), TiO_2 (10 mg), NHPI (0.1 mmol, 16.3 mg), *t*-BuOOH 70% aq. (2 mmol, 257 mg) and a magnetic stir bar (6 × 10 mm) were placed in a 50 mL round-bottom flask. The obtained mixture was sonicated for 5 min in an ultrasonic bath. For the entries of C and D, the flask was vacuumed and then filled with Ar three times. The mixture was magnetically stirred (500 rpm) in a thermostated water bath at 25 °C (±1 °C) under irradiation of 10 W blue LED for 8 h. The conversion of **3aa** was determined by ^1H NMR in MeCN using $C_2H_2Cl_4$ as the internal standard.

3.2. Characterization Data of the Cross-Dehydrogenative C–C Coupling Products

4-Methyl-2-(tetrahydrofuran-2-yl)quinoline 3aa [91] was isolated using column chromatography (Petroleum ether/EtOAc = 2/1) as a colorless viscous liquid (190 mg, 89%).

^{1}H NMR (300.13 MHz, $CDCl_3$) δ 8.07–7.99 (m, 1H), 7.92–7.85 (m, 1H), 7.66–7.58 (m, 1H), 7.48–7.41 (m, 1H), 7.40 (s, 1H), 5.10 (t, *J* = 6.9 Hz, 1H), 4.16–4.08 (m, 1H), 4.02–3.94 (m, 1H), 2.63 (s, 3H), 2.53–2.38 (m, 1H), 2.11–1.90 (m, 3H).^{13}C{^{1}H}NMR (75.48 MHz, $CDCl_3$) δ 163.0, 147.3, 144.8, 129.5, 129.0, 127.4, 125.7, 123.6, 118.6, 82.0, 69.1, 33.2, 25.9, 18.8.

2-(2-hydroperoxytetrahydrofuran-2-yl)-4-methylquinoline 3aa′. ^{13}C{^{1}H}NMR (75.48 MHz, $CDCl_3$) δ 159.4, 146.0, 145.7, 128.8, 128.7, 127.2, 126.1, 123.4, 119.7, 113.3, 69.5, 36.8, 24.8, 19.0. HR-MS (ESI): *m*/*z* = 246.1125, calcd. for $C_{14}H_{15}NO_3$+H^+: 246.1123.

***Anti*-4-methyl-2-(5-methyltetrahydrofuran-2-yl)quinoline 3ab** was isolated using column chromatography (Petroleum ether/EtOAc = 2/1) as a colorless liquid (66 mg, 29%). ^{1}H NMR (300 MHz, Chloroform-*d*) δ 8.07–8.02 (m, 1H), 7.98–7.93 (m, 1H), 7.66 (ddd, *J* = 8.4, 6.8, 1.5 Hz, 1H), 7.50 (ddd, *J* = 8.2, 6.8, 1.3 Hz, 1H), 7.46 (s, 1H), 5.26 (t, *J* = 7.1 Hz, 1H), 4.51–4.33 (m, 1H), 2.70 (s, 3H), 2.63–2.49 (m, 1H), 2.24–2.02 (m, 2H), 1.75–1.59 (m, 1H), 1.36 (d, *J* = 6.1 Hz, 3H). ^{13}C{^{1}H}NMR (75.48 MHz, $CDCl_3$) δ 163.6, 147.3, 145.1, 129.6, 129.2, 127.5, 125.9, 123.8, 118.6, 81.8, 76.7, 34.1, 34.0, 21.5, 19.0; FTIR (KBr): ν_{max} = 2968, 2928, 2869, 1602, 1509, 1447, 1379, 1311, 1225, 1181, 1074, 910, 883, 760 cm^{-1}. HR-MS (ESI): *m*/*z* = 228.1389, calcd. for $C_{15}H_{17}NO$+H^+: 228.1383.

***Syn*-4-methyl-2-(5-methyltetrahydrofuran-2-yl)quinoline 3ab′** was isolated using column chromatography (Petroleum ether/EtOAc = 2/1) as a colorless liquid (59 mg, 26%). ^{1}H NMR (300 MHz, Chloroform-*d*) δ 8.08–8.03 (m, 1H), 7.97 (dd, *J* = 8.4, 1.5 Hz, 1H), 7.68 (ddd, *J* = 8.4, 6.9, 1.5 Hz, 1H), 7.58–7.46 (m, 2H), 5.13 (dd, *J* = 7.6, 6.5 Hz, 1H), 4.33–4.21 (m, 1H), 2.72 (d, *J* = 0.7 Hz, 3H), 2.60–2.42 (m, 1H), 2.21–1.99 (m, 2H), 1.69–1.50 (m, 1H), 1.44 (d, *J* = 6.1 Hz, 3H).^{13}C{^{1}H}NMR (75.48 MHz, $CDCl_3$) δ 163.3, 147.3, 145.2, 129.6, 129.3, 127.6, 126.0, 123.8, 118.8, 82.5, 76.9, 33.5, 33.2, 21.4, 19.1; FTIR (KBr): ν_{max} = 2970, 2928, 2870, 1736, 1602, 1563, 1509, 1447, 1380, 1090, 1032, 913, 882, 760 cm^{-1}. HR-MS (ESI): *m*/*z* = 228.1388, calcd. for $C_{15}H_{17}NO$+H^+: 228.1383.

4-methyl-2-(2-methyltetrahydrofuran-2-yl)quinoline 3ab′ was isolated using column chromatography (Petroleum ether/EtOAc = 2/1) as a colorless liquid (28 mg, 12%). ^{1}H NMR (300 MHz, Chloroform-*d*) δ 8.07 (d, *J* = 8.4, 1H), 7.99–7.94 (m, 1H), 7.67 (ddd, *J* = 8.4, 6.8, 1.5 Hz, 1H), 7.62–7.60 (m, 1H), 7.51 (ddd, *J* = 8.3, 6.9, 1.3 Hz, 1H), 4.13–4.02 (m, 1H), 3.95–3.83 (m, 1H), 2.88–2.75 (m, 1H), 2.71 (d, *J* = 1.0 Hz, 3H), 2.14–1.95 (m, 2H), 1.89–1.74 (m, 1H), 1.65 (s, 3H). ^{13}C{^{1}H}NMR (75.48 MHz, $CDCl_3$) δ 166.6, 147.5, 144.6, 129.9, 129.0, 127.2, 125.8, 123.7, 118.5, 86.2, 68.1, 37.7, 28.3, 26.1, 19.1; FTIR (KBr): ν_{max} = 2977, 2931, 1600, 1447, 1383, 1363, 1196, 1101, 1033, 761 cm^{-1}. HR-MS (ESI): *m*/*z* = 228.1380, calcd. for $C_{15}H_{17}NO$+H^+: 228.1283.

2-(1,3-dioxolan-2-yl)-4-methylquinoline 3ac [65] was isolated using column chromatography (Petroleum ether/EtOAc = 2/1) as a colorless liquid (54 mg, 25%). ^{1}H NMR (500 MHz, Chloroform-*d*) δ 8.16 (d, *J* = 8.4 Hz, 1H), 7.98 (d, *J* = 8.3 Hz, 1H), 7.74–7.67 (m, 1H), 7.59–7.53 (m, 1H), 7.49 (s, 1H), 5.95 (s, 1H), 4.27–4.19 (m, 2H), 4.16–4.08 (m, 2H), 2.71 (s, 3H). ^{13}C{^{1}H}NMR (75.48 MHz, $CDCl_3$) δ 156.7, 147.2, 145.7, 130.2, 129.5, 128.4, 126.9, 123.8, 118.7, 104.3, 65.8, 19.0.

2-(1,3-dioxolan-4-yl)-4-methylquinoline 3ac′ [65] was isolated using column chromatography (Petroleum ether/EtOAc = 2/1) as a colorless liquid (18 mg, 8%). ^{1}H NMR (300 MHz, Chloroform-*d*) δ 8.05 (d, *J* = 8.4 Hz, 1H), 8.00 (dd, *J* = 8.4, 1.4 Hz, 1H), 7.71 (ddd, *J* = 8.4, 6.8, 1.4 Hz, 1H), 7.60–7.52 (m, 1H), 7.48 (s, 1H), 5.34 (s, 1H), 5.33–5.26 (m, 1H), 5.15 (s, 1H), 4.47–4.36 (m, 1H), 4.08 (dd, *J* = 8.3, 5.6 Hz, 1H), 2.73 (s, 3H). ^{13}C{^{1}H}NMR (75.48 MHz, $CDCl_3$) δ 160.0, 147.1, 146.0, 129.7, 129.5, 127.8, 126.5, 123.9, 118.8, 96.4, 78.3, 71.1, 19.1. FTIR (KBr): ν_{max} = 2925, 2855, 16001, 1509, 1449, 1157, 1088, 1029, 936, 760 cm^{-1}. HR-MS (ESI): *m*/*z* = 238.0841, calcd. for $C_{13}H_{13}NO_2$+Na^+: 238.0838.

2-(1,4-dioxan-2-yl)-4-methylquinoline 3ad [85] was isolated using column chromatography (Petroleum ether/EtOAc = 2/1) as white crystals (45 mg, 20%). Mp = 81–82 °C (lit. Mp = 82–83 °C [10.1039/C9OB02653C]). ^{1}H NMR (300 MHz, Chloroform-*d*) δ 8.10 (d, *J* = 8.5 Hz, 1H), 7.98 (d, *J* = 8.7 Hz, 1H), 7.76–7.64 (m, 1H), 7.59–7.51 (m, 1H), 7.47 (s, 1H), 4.92 (dd, *J* = 10.3, 2.9 Hz, 1H), 4.25 (dd, *J* = 11.7, 2.9 Hz, 1H), 4.06–3.94 (m, 2H), 3.88–3.74 (m,

2H), 3.70–3.57 (m, 1H), 2.73 (s, 3H). $^{13}C\{^1H\}$NMR (75.48 MHz, $CDCl_3$) δ 157.9, 147.4, 145.3, 129.9, 129.4, 127.7, 126.3, 123.8, 119.2, 78.9, 71.2, 67.2, 66.5, 18.9.

4-methyl-2-(tetrahydro-2H-pyran-2-yl)quinoline 3ae [85] was isolated using column chromatography (Petroleum ether/EtOAc = 2/1) as a colorless liquid (73 mg, 32%). ^1H NMR (300 MHz, Chloroform-*d*) δ 8.06 (d, *J* = 8.4 Hz, 1H), 7.98–7.89 (m, 1H), 7.70–7.60 (m, 1H), 7.52–7.46 (m, 1H), 7.45 (s, 1H), 4.60 (dd, *J* = 11.0, 2.3 Hz, 1H), 4.25–4.15 (m, 1H), 3.75–3.60 (m, 1H), 2.68 (s, 3H), 2.16–2.04 (m, 1H), 2.03–1.88 (m, 1H), 1.83–1.66 (m, 2H), 1.66–1.51 (m, 2H). $^{13}C\{^1H\}$NMR (75.48 MHz, $CDCl_3$) δ 162.2, 147.2, 145.1, 129.7, 129.1, 127.6, 125.9, 123.7, 118.9, 81.6, 68.9, 32.8, 25.9, 23.8, 18.9.

2-(1-ethoxyethyl)-4-methylquinoline 3af [85] was isolated using column chromatography (CH_2Cl_2/EtOAc = 20/1) as a colorless liquid (77 mg, 36%). ^1H NMR (300 MHz, Chloroform-*d*) δ 8.07 (d, *J* = 8.4 Hz, 1H), 7.97 (d, *J* = 8.3 Hz, 1H), 7.68 (t, *J* = 8.4 Hz, 1H), 7.57–7.48 (m, 1H), 7.44 (s, 1H), 4.69 (q, *J* = 6.6 Hz, 1H), 3.57– 3.45 (m, 1H), 3.47–3.34 (m, 1H), 2.72 (s, 3H), 1.53 (d, *J* = 6.6 Hz, 3H), 1.22 (t, *J* = 7.1 Hz, 3H).$^{13}C\{^1H\}$NMR (75.48 MHz, $CDCl_3$) δ 164.1, 147.2, 145.5, 129.6, 129.3, 127.8, 126.1, 123.8, 118.4, 79.7, 64.8, 22.7, 19.1, 15.6

2-methoxy-4-(tetrahydrofuran-2-yl)quinoline 3ba was isolated using column chromatography (EtOAc/petroleum ether 1/2) as a colorless liquid (122 mg, 53%). ^1H NMR (300 MHz, Chloroform-*d*) δ 7.89 (d, *J* = 8.4 Hz, 1H), 7.81–7.72 (m, 1H), 7.68–7.54 (m, 1H), 7.44–7.31 (m, 1H), 7.07 (s, 1H), 5.52 (t, *J* = 6.9 Hz, 1H), 4.27–4.13 (m, 1H), 4.08 (s, 3H), 4.08–3.95 (m, 1H), 2.65–2.47 (m, 1H), 2.14–1.92 (m, 2H), 1.92–1.78 (m, 1H). $^{13}C\{^1H\}$NMR (75.48 MHz, $CDCl_3$) δ 162.8, 152.3, 147.1, 129.2, 128.1, 123.8, 123.3, 122.9, 108.5, 76.8, 69.1, 53.4, 33.7, 26.0. FTIR (KBr): ν_{max} = 2979, 2949, 1612, 1575, 1473, 1438, 1387, 1366, 1340, 1238, 1195, 1080, 1055, 1024, 761 cm^{-1}. HR-MS (ESI): *m*/*z* = 230.1181, calcd. for $C_{14}H_{15}NO_2$+H^+: 230.1176

2-chloro-4-(tetrahydrofuran-2-yl)quinoline 3ca was isolated using column chromatography (Petroleum ether/EtOAc = 2/1) as a slightly yellow liquid (87 mg, 37%). ^1H NMR (300.13 MHz, $CDCl_3$) δ 8.04 (d, *J* = 8.5 Hz, 1H), 7.85 (dd, *J* = 8.4, 1.4 Hz, 1H), 7.71 (ddd, *J* = 8.4, 6.9, 1.4 Hz, 1H), 7.60–7.49 (m, 1H), 7.54 (s, 1H), 5.55 (t, *J* = 7.1 Hz, 1H), 4.22 (m, 1H), 4.02 (m, 1H), 2.70–2.55 (m, 1H), 2.13–1.95 (m, 2H), 1.94–1.76 (m, 1H).$^{13}C\{^1H\}$NMR (75.48 MHz, $CDCl_3$) δ 153.1, 151.4, 148.1, 130.2, 129.5, 126.8, 124.5, 123.4, 117.9, 76.7, 69.2, 34.0, 26.1. FTIR (KBr): ν_{max} = 2965, 2928, 2871, 1586, 1560, 1506, 1292, 1264, 1145, 1099, 1081, 1041, 1021, 878, 855, 792, 763 cm^{-1}. HR-MS (ESI): *m*/*z* = 234.0688, calcd. for $C_{13}H_{12}ClNO$+H^+: 234.0680.

2-methyl-4-(tetrahydrofuran-2-yl)quinoline 3ea [91] was isolated using column chromatography (Petroleum ether/EtOAc = 2/1) as a colorless liquid (161 mg, 75%). ^1H NMR (300 MHz, Chloroform-*d*) δ 8.03 (d, *J* = 8.3 Hz, 1H), 7.81 (d, *J* = 8.4 Hz, 1H), 7.69–7.57 (m, 1H), 7.50–7.41 (m, 1H), 7.42 (s, 1H), 5.53 (t, *J* = 7.1 Hz, 1H), 4.24–4.14 (m, 1H), 4.00 (q, *J* = 7.1 Hz, 1H), 2.65–2.47 (m, 1H), 2.12–1.89 (m, 2H), 1.86–1.72 (m, 1H). $^{13}C\{^1H\}$NMR (75.48 MHz, $CDCl_3$) δ 159.1, 149.4, 147.9, 129.4, 129.0, 125.5, 123.9, 123.0, 117.2, 76.8, 69.0, 33.9, 26.0, 25.6.

2-(tetrahydrofuran-2-yl)quinoxaline 3fa [66] was isolated using column chromatography (Petroleum ether/EtOAc = 2/1) as a colorless liquid (113 mg, 56%). ^1H NMR (300.13 MHz, $CDCl_3$) δ 9.02 (s, 1H), 8.12–8.07 (m, 1H), 8.07–8.01 (m, 1H), 7.76–7.69 (m, 2H), 5.21 (t, *J* = 7.0 Hz, 1H), 4.17 (q, *J* = 7.0 Hz, 1H), 4.05 (dd, *J* = 7.2 Hz, 1H), 2.57–2.46 (m, 1H), 2.21–2.11 (m, 1H), 2.11–2.00 (m, 2H). $^{13}C\{^1H\}$NMR (75.48 MHz, $CDCl_3$) δ 157.7, 143.6, 142.0, 141.7, 130.2, 129.6, 129.3, 129.2, 80.6, 69.5, 33.0, 26.1.

2-(tetrahydrofuran-2-yl)pyrazine 3ga was isolated using column chromatography (CH_2Cl_2/MeOH = 50/1) as a colorless liquid (59 mg, 40%).^1H NMR (300 MHz, Chloroform-*d*) δ 8.68 (s, 1H), 8.52–8.36 (m, 2H), 5.01 (t, *J* = 6.4 Hz, 1H), 4.14–4.02 (m, 1H), 4.00–3.87 (m, 1H), 2.49–2.29 (m, 1H), 2.11–1.86 (m, 3H). $^{13}C\{^1H\}$NMR (75.48 MHz, $CDCl_3$) δ 158.2, 143.8, 143.5, 142.7, 79.8, 69.3, 32.9, 25.9. FTIR (KBr): ν_{max} = 3389, 2959, 2882, 1724, 1701, 1406, 1304, 1140, 1052, 1020 cm^{-1}. HR-MS (ESI): *m*/*z* = 151.0873, calcd. for $C_8H_{10}N_2O$+H^+: 151.0866.

2-methyl-3-(tetrahydrofuran-2-yl)pyrazine 3ha was isolated using column chromatography (CH_2Cl_2/MeOH = 50/1) as a slightly yellow liquid (76 mg, 46%).^1H NMR (300 MHz, Chloroform-*d*) δ 8.37 (d, *J* = 2.6 Hz, 1H), 8.34 (d, *J* = 2.6 Hz, 1H), 5.15 (t, *J* = 7.0 Hz, 1H), 4.13–4.04 (m, 1H), 3.99–3.89 (m, 1H), 2.63 (s, 3H), 2.31–2.19 (m, 2H), 2.17–1.96 (m, 2H).

$^{13}C\{^1H\}$NMR (75.48 MHz, $CDCl_3$) δ 154.5, 152.5, 142.6, 141.5, 78.3, 69.2, 30.4, 26.3, 21.6. FTIR (KBr): ν_{max} = 3240, 3051, 2959, 2878, 1774, 1726, 1701, 1405, 1299, 1169, 1130, 1105, 1055, 988, 923, 857, 732 cm^{-1}. HR-MS (ESI): m/z = 165.1023, calcd. for $C_9H_{10}N_2O+H^+$: 165.1022.

Methyl 6-(tetrahydrofuran-2-yl)nicotinate 3ia [91] was isolated using column chromatography (EtOAc/DCM = 1/20→1/5) as an orange liquid (119 mg, 57%). ^1H NMR (300.13 MHz, $CDCl_3$) δ 9.11 (d, *J* = 2.2 Hz, 1H), 8.25 (dd, *J* = 8.2, 2.2 Hz, 1H), 7.52 (d, *J* = 8.2 Hz, 1H), 5.11–4.95 (m, 1H), 4.32–3.74 (m, 5H), 2.57–2.33 (m, 1H), 2.09–1.81 (m, 3H). $^{13}C\{^1H\}$NMR (75.48 MHz, $CDCl_3$) δ 167.8, 165.9, 150.4, 137.9, 124.6, 119.4, 81.2, 69.3, 52.4, 33.2, 25.8.

4-methyl-2-(tetrahydrofuran-2-yl)quinoline 1-oxide 3ja [76] was isolated using column chromatography (Petroleum ether/EtOAc = 2/1) as a colorless liquid (78 mg, 34%). ^1H NMR (300 MHz, Chloroform-*d*) δ 8.81–8.74 (m, 1H), 7.99–7.92 (m, 1H), 7.80–7.71 (m, 1H), 7.67–7.59 (m, 1H), 7.44 (s, 1H), 5.58 (t, *J* = 6.7 Hz, 1H), 4.17 (q, *J* = 6.9 Hz, 1H), 4.02 (q, *J* = 7.1 Hz, 1H), 2.90–2.76 (m, 1H), 2.68 (s, 3H), 2.13–1.98 (m, 1H), 1.99–1.82 (m, 2H). $^{13}C\{^1H\}$NMR (75.48 MHz, $CDCl_3$) δ 150.8, 141.1, 135.4, 130.3, 128.8, 128.0, 124.8, 119.9, 118.9, 76.1, 69.5, 31.2, 26.0, 18.6.

1-(tetrahydrofuran-2-yl)isoquinoline 3ka [91] was isolated using column chromatography (CH_2Cl_2/EtOAc from 5/1 to 5/2) as a colorless liquid (130 mg, 65%). ^1H NMR (300.13 MHz, $CDCl_3$) δ 8.50 (d, *J* = 5.8 Hz, 1H), 8.34 (d, *J* = 8.3 Hz, 1H), 7.82 (d, *J* = 8.1 Hz, 1H), 7.75–7.52 (m, 3H), 5.72 (t, *J* = 7.1 Hz, 1H), 4.20 (q, *J* = 7.3 Hz, 1H), 4.03 (q, *J* = 7.5 Hz, 1H), 2.60–2.32 (m, 2H), 2.27–2.01 (m, 2H).$^{13}C\{^1H\}$NMR (75.48 MHz, $CDCl_3$) δ 159.7, 141.4, 136.7, 130.1, 127.5, 127.3, 126.7, 125.5, 120.7, 79.2, 69.1, 30.9, 26.3.

2-(4-bromophenyl)imidazo [1,2-a]pyridine-3-carboxylic acid 3la' [106] was isolated using column chromatography (CH_2Cl_2/EtOAc = 5/2) as slightly yellow crystals (82 mg, 30%). ^1H NMR (300 MHz, Chloroform-*d*) δ 9.27 (bs, 1H, NH), 8.41 (d, *J* = 8.4 Hz, 1H), 8.28–8.19 (m, 1H), 7.84 (d, *J* = 8.5 Hz, 2H), 7.81–7.74 (m, 1H), 7.62 (d, *J* = 8.5 Hz, 2H), 7.09 (dd, *J* = 7.3, 4.9 Hz, 1H). $^{13}C\{^1H\}$NMR (75.48 MHz, $CDCl_3$) δ 165.1, 151.5, 147.1, 139.3, 133.1, 132.2, 129.2, 127.4, 120.2, 114.8.

4. Conclusions

In this work, a new visible-light active heterogeneous photocatalyst system based on industrially available and non-toxic TiO_2 and NHPI was proposed for the cross-dehydrogenative C–C coupling of electron-deficient N-heterocycles with ethers. In this photocatalytic system, phthalimide-*N*-oxyl radicals photogenerated on the surface of titanium oxide become active mediators of the reaction, which leads to 1) an increase in efficiency due to the homogeneous organocatalytic process in solution and 2) allows the selective cleavage of the weak CH bonds. We have proposed a new mild method for the generation of C-centered radicals from non-activated esters for the Minisci reaction. Despite the fact that acidic additives are frequently used in Minisci-type reactions, the addition of acid was not necessary in our procedure in the case of several substrates. Optimal conditions were chosen for the Minisci reaction between π-deficient pyridine, quinoline, pyrazine, and quinoxaline heteroarenes with non-activated ethers.

Supplementary Materials: The following supporting information can be downloaded at: https://www.mdpi.com/article/10.3390/molecules28030934/s1, copies of NMR spectra of the synthesized products, the comparison of the developed method with the literature procedure, the determination of the side products of the studied reaction.

Author Contributions: Conceptualization, I.B.K.; methodology, I.B.K. and E.R.L.; investigation, E.R.L., O.O.S., V.M.M. and A.I.I.; writing—original draft preparation, E.R.L.; writing—review and editing, I.B.K. and A.O.T.; supervision, I.B.K. and A.O.T.; project administration, I.B.K. All authors have read and agreed to the published version of the manuscript.

Funding: This research received no external funding.

Institutional Review Board Statement: Not applicable.

Informed Consent Statement: Not applicable.

Data Availability Statement: Not applicable.

Acknowledgments: We are grateful to the Department of Structural Studies, Zelinsky Institute of Organic Chemistry for the HRMS analysis.

Conflicts of Interest: The authors declare no conflict of interest.

Sample Availability: Not applicable.

References

1. Friedmann, D.; Hakki, A.; Kim, H.; Choi, W.; Bahnemann, D. Heterogeneous Photocatalytic Organic Synthesis: State-of-the-Art and Future Perspectives. *Green Chem.* **2016**, *18*, 5391–5411. [CrossRef]
2. Xiao, J.; Liu, X.; Pan, L.; Shi, C.; Zhang, X.; Zou, J.-J. Heterogeneous Photocatalytic Organic Transformation Reactions Using Conjugated Polymers-Based Materials. *ACS Catal.* **2020**, *10*, 12256–12283. [CrossRef]
3. Kohtani, S.; Kawashima, A.; Miyabe, H. Stereoselective Organic Reactions in Heterogeneous Semiconductor Photocatalysis. *Front. Chem.* **2019**, *7*, 630. [CrossRef] [PubMed]
4. Verma, S.K.; Verma, R.; Girish, Y.R.; Xue, F.; Yan, L.; Verma, S.; Singh, M.; Vaishnav, Y.; Shaik, A.B.; Bhandare, R.R.; et al. Heterogeneous Graphitic Carbon Nitrides in Visible-Light-Initiated Organic Transformations. *Green Chem.* **2022**, *24*, 438–479. [CrossRef]
5. Chen, J.; Cen, J.; Xu, X.; Li, X. The Application of Heterogeneous Visible Light Photocatalysts in Organic Synthesis. *Catal. Sci. Technol.* **2016**, *6*, 349–362. [CrossRef]
6. Li, F.; Cheng, L.; Fan, J.; Xiang, Q. Steering the Behavior of Photogenerated Carriers in Semiconductor Photocatalysts: A New Insight and Perspective. *J. Mater. Chem. A* **2021**, *9*, 23765–23782. [CrossRef]
7. Wang, H.; Zhang, L.; Chen, Z.; Hu, J.; Li, S.; Wang, Z.; Liu, J.; Wang, X. Semiconductor Heterojunction Photocatalysts: Design, Construction, and Photocatalytic Performances. *Chem. Soc. Rev.* **2014**, *43*, 5234. [CrossRef] [PubMed]
8. Miyauchi, M.; Irie, H.; Liu, M.; Qiu, X.; Yu, H.; Sunada, K.; Hashimoto, K. Visible-Light-Sensitive Photocatalysts: Nanocluster-Grafted Titanium Dioxide for Indoor Environmental Remediation. *J. Phys. Chem. Lett.* **2016**, *7*, 75–84. [CrossRef] [PubMed]
9. Ahmed, S.N.; Haider, W. Heterogeneous Photocatalysis and Its Potential Applications in Water and Wastewater Treatment: A Review. *Nanotechnology* **2018**, *29*, 342001. [CrossRef]
10. Thambiliyagodage, C. Activity Enhanced TiO_2 Nanomaterials for Photodegradation of Dyes—A Review. *Environ. Nanotechnol. Monit. Manag.* **2021**, *16*, 100592. [CrossRef]
11. Marchuk, M.V.; Asanov, I.P.; Panafidin, M.A.; Vorotnikov, Y.A.; Shestopalov, M.A. Nano TiO_2 and Molybdenum/Tungsten Iodide Octahedral Clusters: Synergism in UV/Visible-Light Driven Degradation of Organic Pollutants. *Nanomaterials* **2022**, *12*, 4282. [CrossRef]
12. Stavitskaya, A.; Glotov, A.; Pouresmaeil, F.; Potapenko, K.; Sitmukhanova, E.; Mazurova, K.; Ivanov, E.; Kozlova, E.; Vinokurov, V.; Lvov, Y. CdS Quantum Dots in Hierarchical Mesoporous Silica Templated on Clay Nanotubes: Implications for Photocatalytic Hydrogen Production. *ACS Appl. Nano Mater.* **2022**, *5*, 605–614. [CrossRef]
13. Kurenkova, A.Y.; Medvedeva, T.B.; Gromov, N.V.; Bukhtiyarov, A.V.; Gerasimov, E.Y.; Cherepanova, S.V.; Kozlova, E.A. Sustainable Hydrogen Production from Starch Aqueous Suspensions over a $Cd_{0.7}Zn_{0.3}S$-Based Photocatalyst. *Catalysts* **2021**, *11*, 870. [CrossRef]
14. Kozlova, E.A.; Lyulyukin, M.N.; Kozlov, D.V.; Parmon, V.N. Semiconductor Photocatalysts and Mechanisms of Carbon Dioxide Reduction and Nitrogen Fixation under UV and Visible Light. *Russ. Chem. Rev.* **2021**, *90*, 1520–1543. [CrossRef]
15. Wang, J.; Guo, R.; Bi, Z.; Chen, X.; Hu, X.; Pan, W. A Review on TiO_{2-x}-Based Materials for Photocatalytic CO_2 Reduction. *Nanoscale* **2022**, *14*, 11512–11528. [CrossRef]
16. Shtyka, O.; Shatsila, V.; Ciesielski, R.; Kedziora, A.; Maniukiewicz, W.; Dubkov, S.; Gromov, D.; Tarasov, A.; Rogowski, J.; Stadnichenko, A.; et al. Adsorption and Photocatalytic Reduction of Carbon Dioxide on TiO_2. *Catalysts* **2020**, *11*, 47. [CrossRef]
17. Eidsvåg, H.; Bentouba, S.; Vajeeston, P.; Yohi, S.; Velauthapillai, D. TiO_2 as a Photocatalyst for Water Splitting—An Experimental and Theoretical Review. *Molecules* **2021**, *26*, 1687. [CrossRef]
18. Bian, Y.; Gu, Y.; Zhang, X.; Chen, H.; Li, Z. Engineering $BiOBr_xI_{1-x}$ Solid Solutions with Enhanced Singlet Oxygen Production for Photocatalytic Benzylic C-H Bond Activation Mediated by N-Hydroxyl Compounds. *Chin. Chem. Lett.* **2021**, *32*, 2837–2840. [CrossRef]
19. Shi, G.; Xu, S.; Bao, Y.; Xu, J.; Liang, Y. Selective Aerobic Oxidation of Toluene to Benzaldehyde on Immobilized CoO_x on SiO_2 Catalyst in the Presence of N-Hydroxyphthalimide and Hexafluoropropan-2-Ol. *Catal. Commun.* **2019**, *123*, 73–78. [CrossRef]
20. Krylov, I.B.; Lopat'eva, E.R.; Subbotina, I.R.; Nikishin, G.I.; Yu, B.; Terent'ev, A.O. Mixed Hetero-/Homogeneous TiO_2/N-Hydroxyimide Photocatalysis in Visible-Light-Induced Controllable Benzylic Oxidation by Molecular Oxygen. *Chin. J. Catal.* **2021**, *42*, 1700–1711. [CrossRef]
21. Wang, Y.; Wang, X.; Antonietti, M. Polymeric Graphitic Carbon Nitride as a Heterogeneous Organocatalyst: From Photochemistry to Multipurpose Catalysis to Sustainable Chemistry. *Angew. Chem. Int. Ed.* **2012**, *51*, 68–89. [CrossRef] [PubMed]

22. Hao, H.; Shi, J.-L.; Xu, H.; Li, X.; Lang, X. N-Hydroxyphthalimide-TiO_2 Complex Visible Light Photocatalysis. *Appl. Catal. B: Environ.* **2019**, *246*, 149–155. [CrossRef]
23. Li, H.; Li, X.; Lang, X. Extending the π-Conjugated Molecules on TiO_2 for the Selective Photocatalytic Aerobic Oxidation of Sulfides Triggered by Visible Light. *Sustain. Energy Fuels* **2021**, *5*, 2127–2135. [CrossRef]
24. Bhat, V.T.; Duspara, P.A.; Seo, S.; Abu Bakar, N.S.B.; Greaney, M.F. Visible Light Promoted Thiol-Ene Reactions Using Titanium Dioxide. *Chem. Commun.* **2015**, *51*, 4383–4385. [CrossRef]
25. Park, S.; Jeong, J.; Fujita, K.; Yamamoto, A.; Yoshida, H. Anti-Markovnikov Hydroamination of Alkenes with Aqueous Ammonia by Metal-Loaded Titanium Oxide Photocatalyst. *J. Am. Chem. Soc.* **2020**, *142*, 12708–12714. [CrossRef]
26. Manley, D.W.; Walton, J.C. A Clean and Selective Radical Homocoupling Employing Carboxylic Acids with Titania Photoredox Catalysis. *Org. Lett.* **2014**, *16*, 5394–5397. [CrossRef]
27. Manley, D.W.; McBurney, R.T.; Miller, P.; Walton, J.C.; Mills, A.; O'Rourke, C. Titania-Promoted Carboxylic Acid Alkylations of Alkenes and Cascade Addition–Cyclizations. *J. Org. Chem.* **2014**, *79*, 1386–1398. [CrossRef]
28. Zhu, Q.; Nocera, D.G. Photocatalytic Hydromethylation and Hydroalkylation of Olefins Enabled by Titanium Dioxide Mediated Decarboxylation. *J. Am. Chem. Soc.* **2020**, *142*, 17913–17918. [CrossRef]
29. Savateev, A.; Ghosh, I.; König, B.; Antonietti, M. Photoredox Catalytic Organic Transformations Using Heterogeneous Carbon Nitrides. *Angew. Chem. Int. Ed.* **2018**, *57*, 15936–15947. [CrossRef]
30. Bianchi, P.; Williams, J.D.; Kappe, C.O. Continuous Flow Processing of Bismuth-Photocatalyzed Atom Transfer Radical Addition Reactions Using an Oscillatory Flow Reactor. *Green Chem.* **2021**, *23*, 2685–2693. [CrossRef]
31. Ghosh, I.; Khamrai, J.; Savateev, A.; Shlapakov, N.; Antonietti, M.; König, B. Organic Semiconductor Photocatalyst Can Bifunctionalize Arenes and Heteroarenes. *Science* **2019**, *365*, 360–366. [CrossRef]
32. Wang, J.; Su, P.; Abdolmohammadi, S.; Vessally, E. A Walk around the Application of Nanocatalysts for Cross-Dehydrogenative Coupling of C–H Bonds. *RSC Adv.* **2019**, *9*, 41684–41702. [CrossRef] [PubMed]
33. Buglioni, L.; Riente, P.; Palomares, E.; Pericàs, M.A. Visible-Light-Promoted Arylation Reactions Photocatalyzed by Bismuth(III) Oxide: Visible-Light-Promoted Arylation Reactions Photocatalyzed by Bismuth(III) Oxide. *Eur. J. Org. Chem.* **2017**, *2017*, 6986–6990. [CrossRef]
34. Franchi, D.; Amara, Z. Applications of Sensitized Semiconductors as Heterogeneous Visible-Light Photocatalysts in Organic Synthesis. *ACS Sustain. Chem. Eng.* **2020**, *8*, 15405–15429. [CrossRef]
35. Peiris, S.; Silva, H.B.; Ranasinghe, K.N.; Bandara, S.V.; Perera, I.R. Recent Development and Future Prospects of TiO_2 Photocatalysis. *J. Chin. Chem. Soc.* **2021**, *68*, 738–769. [CrossRef]
36. Arora, I.; Chawla, H.; Chandra, A.; Sagadevan, S.; Garg, S. Advances in the Strategies for Enhancing the Photocatalytic Activity of TiO_2: Conversion from UV-Light Active to Visible-Light Active Photocatalyst. *Inorg. Chem. Commun.* **2022**, *143*, 109700. [CrossRef]
37. Basavarajappa, P.S.; Patil, S.B.; Ganganagappa, N.; Reddy, K.R.; Raghu, A.V.; Reddy, C.V. Recent Progress in Metal-Doped TiO_2, Non-Metal Doped/Codoped TiO_2 and TiO_2 Nanostructured Hybrids for Enhanced Photocatalysis. *Int. J. Hydrogen Energy* **2020**, *45*, 7764–7778. [CrossRef]
38. Zani, L.; Melchionna, M.; Montini, T.; Fornasiero, P. Design of Dye-Sensitized TiO_2 Materials for Photocatalytic Hydrogen Production: Light and Shadow. *J. Phys. Energy* **2021**, *3*, 031001. [CrossRef]
39. Choi, S.K.; Yang, H.S.; Kim, J.H.; Park, H. Organic Dye-Sensitized TiO_2 as a Versatile Photocatalyst for Solar Hydrogen and Environmental Remediation. *Appl. Catal. B Environ.* **2012**, *121–122*, 206–213. [CrossRef]
40. Gorduk, S.; Avciata, O.; Avciata, U. Hydrothermal in Situ Preparation of Phthalocyanine–TiO_2 Nanocomposites for Photocatalytic Activity under Visible Light Irradiation. *Res. Chem. Intermed.* **2021**, *47*, 615–635. [CrossRef]
41. Zhou, X.; Wang, X.; Li, J.; Zhang, X. Enhanced Photocatalytic Activity in Metal Phthalocyanine-Sensitized TiO_2 Nanorods. *Res. Chem. Intermed.* **2021**, *47*, 1519–1533. [CrossRef]
42. Yang, L.; Li, L.; Li, L.; Liu, C.; Li, J.; Lai, B.; Li, N. N/Fe/Zn Co-Doped TiO_2 Loaded on Basalt Fiber with Enhanced Photocatalytic Activity for Organic Pollutant Degradation. *RSC Adv.* **2021**, *11*, 4942–4951. [CrossRef] [PubMed]
43. Wafi, A.; Szabó-Bárdos, E.; Horváth, O.; Makó, É.; Jakab, M.; Zsirka, B. Coumarin-Based Quantification of Hydroxyl Radicals and Other Reactive Species Generated on Excited Nitrogen-Doped TiO_2. *J. Photochem. Photobiol. A Chem.* **2021**, *404*, 112913. [CrossRef]
44. Gui, Q.-W.; Teng, F.; Yu, P.; Wu, Y.-F.; Nong, Z.-B.; Yang, L.-X.; Chen, X.; Yang, T.-B.; He, W.-M. Visible Light-Induced Z-Scheme V_2O_5/g-C_3N_4 Heterojunction Catalyzed Cascade Reaction of Unactivated Alkenes. *Chin. J. Catal.* **2023**, *44*, 111–116. [CrossRef]
45. Khan, S.; Sadiq, M.; Kim, D.; Ullah, M.; Muhammad, N. TiO_2 and Its Binary $ZnTiO_2$ and Ternary $CdZnTiO_2$ Nanocomposites as Efficient Photocatalysts for the Organic Dyes Degradation. *Appl. Water Sci.* **2022**, *12*, 118. [CrossRef]
46. Wu, J.; Ou, P.; Lin, Y.; Tan, X.; Wei, F.; Mi, Y.; Liu, S.; Huang, K. Oxygen Vacancies and Bi_2S_3 Nanoparticles Co-Sensitized TiO_2 Nanotube Arrays for Enhanced Photoelectrochemical Sensing of Chlorpyrifos. *J. Electroanal. Chem.* **2022**, *911*, 116220. [CrossRef]
47. Liu, S.; Zou, Q.; Ma, Y.; Chi, D.; Chen, R.; Fang, H.; Hu, W.; Zhang, K.; Chen, L.-F. Metal-Organic Frameworks Derived TiO_2/Carbon Nitride Heterojunction Photocatalyst with Efficient Catalytic Performance under Visible Light. *Inorg. Chim. Acta* **2022**, *536*, 120918. [CrossRef]
48. Shawky, A.; Alahmadi, N.; Mohamed, R.M.; Zaki, Z.I. Bi_2S_3-Sensitized TiO_2 Nanostructures Prepared by Solution Process for Highly Efficient Photoreduction of Hexavalent Chromium Ions in Water under Visible Light. *Opt. Mater.* **2022**, *124*, 111964. [CrossRef]

49. Cipagauta-Díaz, S.; Estrella-González, A.; Navarrete-Magaña, M.; Gómez, R. N Doped -TiO_2 Coupled to $BiVO_4$ with High Performance in Photodegradation of Ofloxacin Antibiotic and Rhodamine B Dye under Visible Light. *Catal. Today* **2022**, *394–396*, 445–457. [CrossRef]
50. Rajh, T.; Nedeljkovic, J.M.; Chen, L.X.; Poluektov, O.; Thurnauer, M.C. Improving Optical and Charge Separation Properties of Nanocrystalline TiO_2 by Surface Modification with Vitamin C. *J. Phys. Chem. B* **1999**, *103*, 3515–3519. [CrossRef]
51. Sredojević, D.N.; Kovač, T.; Džunuzović, E.; Đorđević, V.; Grgur, B.N.; Nedeljković, J.M. Surface-Modified TiO_2 Powders with Phenol Derivatives: A Comparative DFT and Experimental Study. *Chem. Phys. Lett.* **2017**, *686*, 167–172. [CrossRef]
52. Zhang, T.; Wojtal, P.; Rubel, O.; Zhitomirsky, I. Density Functional Theory and Experimental Studies of Caffeic Acid Adsorption on Zinc Oxide and Titanium Dioxide Nanoparticles. *RSC Adv.* **2015**, *5*, 106877–106885. [CrossRef]
53. Higashimoto, S.; Nishi, T.; Yasukawa, M.; Azuma, M.; Sakata, Y.; Kobayashi, H. Photocatalysis of Titanium Dioxide Modified by Catechol-Type Interfacial Surface Complexes (ISC) with Different Substituted Groups. *J. Catal.* **2015**, *329*, 286–290. [CrossRef]
54. Moongraksathum, B.; Hsu, P.-T.; Chen, Y.-W. Photocatalytic Activity of Ascorbic Acid-Modified TiO_2 Sol Prepared by the Peroxo Sol–Gel Method. *J. Sol-Gel Sci. Technol.* **2016**, *78*, 647–659. [CrossRef]
55. Fujisawa, J.; Matsumura, S.; Hanaya, M. A Single Ti-O-C Linkage Induces Interfacial Charge-Transfer Transitions between TiO_2 and a π-Conjugated Molecule. *Chem. Phys. Lett.* **2016**, *657*, 172–176. [CrossRef]
56. Bui, H.T.; Park, H.Y.; Alvarez, P.J.J.; Lee, J.; Kim, W.; Kim, E.-J. Visible-Light Activation of a Dissolved Organic Matter–TiO_2 Complex Mediated via Ligand-to-Metal Charge Transfer. *Environ. Sci. Technol.* **2022**, *56*, 10829–10837. [CrossRef] [PubMed]
57. Terent'ev, A.O.; Krylov, I.B.; Sharipov, M.Y.; Kazanskaya, Z.M.; Nikishin, G.I. Generation and Cross-Coupling of Benzyl and Phthalimide-N-Oxyl Radicals in a Cerium(IV) Ammonium Nitrate/N-Hydroxyphthalimide/$ArCH_2R$ System. *Tetrahedron* **2012**, *68*, 10263–10271. [CrossRef]
58. Terent'ev, A.O.; Krylov, I.B.; Timofeev, V.P.; Starikova, Z.A.; Merkulova, V.M.; Ilovaisky, A.I.; Nikishin, G.I. Oxidative C-O Cross-Coupling of 1,3-Dicarbonyl Compounds and Their Heteroanalogues with *N* -Substituted Hydroxamic Acids and *N* -Hydroxyimides. *Adv. Synth. Catal.* **2013**, *355*, 2375–2390. [CrossRef]
59. Krylov, I.B.; Lopat'eva, E.R.; Budnikov, A.S.; Nikishin, G.I.; Terent'ev, A.O. Metal-Free Cross-Dehydrogenative C–O Coupling of Carbonyl Compounds with *N* -Hydroxyimides: Unexpected Selective Behavior of Highly Reactive Free Radicals at an Elevated Temperature. *J. Org. Chem.* **2020**, *85*, 1935–1947. [CrossRef] [PubMed]
60. Kammer, L.; Rahman, A.; Opatz, T. A Visible Light-Driven Minisci-Type Reaction with N-Hydroxyphthalimide Esters. *Molecules* **2018**, *23*, 764. [CrossRef]
61. Fiorati, A.; Gambarotti, C.; Melone, L.; Pastori, N.; Punta, C.; Raffaini, G.; Truscello, A. Recent Advances in Photocatalytic Minisci Reaction: An Eco-Friendly Functionalization of Biologically Relevant Heteroarenes. In *Green Synthetic Approaches for Biologically Relevant Heterocycles*; Elsevier: Amsterdam, The Netherlands, 2021; pp. 189–206, ISBN 978-0-12-820586-0.
62. Proctor, R.S.J.; Phipps, R.J. Recent Advances in Minisci-Type Reactions. *Angew. Chem. Int. Ed.* **2019**, *58*, 13666–13699. [CrossRef] [PubMed]
63. Minisci, F.; Bernardi, R.; Bertini, F.; Galli, R.; Perchinummo, M. Nucleophilic Character of Alkyl Radicals—VI. *Tetrahedron* **1971**, *27*, 3575–3579. [CrossRef]
64. Duncton, M.A.J. Minisci Reactions: Versatile CH-Functionalizations for Medicinal Chemists. *Med. Chem. Commun.* **2011**, *2*, 1135. [CrossRef]
65. Fontana, F.; Minisci, F.; Yong, M.Y.; Lihua, Z. A Novel and Mild Source of Carbon-Centered Radicals by Iodosobenzene Diacetate (IBDA) and Sodium Azide from Alcohols, Ethers, Aldehydes, Amides and Alkyl Iodides. *Tetrahedron Lett.* **1993**, *34*, 2517–2520. [CrossRef]
66. Devari, S.; Shah, B.A. Visible Light-Promoted C–H Functionalization of Ethers and Electron-Deficient Arenes. *Chem. Commun.* **2016**, *52*, 1490–1493. [CrossRef] [PubMed]
67. Tauber, J.; Imbri, D.; Opatz, T. Radical Addition to Iminium Ions and Cationic Heterocycles. *Molecules* **2014**, *19*, 16190–16222. [CrossRef]
68. McCallum, T.; Jouanno, L.-A.; Cannillo, A.; Barriault, L. Persulfate-Enabled Direct C–H Alkylation of Heteroarenes with Unactivated Ethers. *Synlett* **2016**, *27*, 1282–1286. [CrossRef]
69. Chupakhin, O.N.; Charushin, V.N. Recent Advances in the Field of Nucleophilic Aromatic Substitution of Hydrogen. *Tetrahedron Lett.* **2016**, *57*, 2665–2672. [CrossRef]
70. Charushin, V.N.; Chupakhin, O.N. Nucleophilic C—H Functionalization of Arenes: A Contribution to Green Chemistry. *Russ. Chem. Bull.* **2019**, *68*, 453–471. [CrossRef]
71. Akulov, A.A.; Varaksin, M.V.; Mampuys, P.; Charushin, V.N.; Chupakhin, O.N.; Maes, B.U.W. C(Sp^2)–H Functionalization in Non-Aromatic Azomethine-Based Heterocycles. *Org. Biomol. Chem.* **2021**, *19*, 297–312. [CrossRef]
72. Liu, X.-L.; Jiang, L.-B.; Luo, M.-P.; Ren, Z.; Wang, S.-G. Recent Advances in Catalytic Enantioselective Direct C–H Bond Functionalization of Electron-Deficient N-Containing Heteroarenes. *Org. Chem. Front.* **2022**, *9*, 265–280. [CrossRef]
73. Jeong, J.; Patel, P.; Hwang, H.; Chang, S. Rhodium(III)-Catalyzed C–C Bond Formation of Quinoline *N*-Oxides at the C-8 Position under Mild Conditions. *Org. Lett.* **2014**, *16*, 4598–4601. [CrossRef]
74. Sharma, U.; Park, Y.; Chang, S. Rh(III)-Catalyzed Traceless Coupling of Quinoline *N*-Oxides with Internal Diarylalkynes. *J. Org. Chem.* **2014**, *79*, 9899–9906. [CrossRef] [PubMed]

75. Zhang, X.; Qi, Z.; Li, X. Rhodium(III)-Catalyzed C-C and C-O Coupling of Quinoline *N*-Oxides with Alkynes: Combination of C-H Activation with O-Atom Transfer. *Angew. Chem.* **2014**, *126*, 10970–10974. [CrossRef]
76. Wu, Z.; Pi, C.; Cui, X.; Bai, J.; Wu, Y. Direct C-2 Alkylation of Quinoline *N*-Oxides with Ethers via Palladium-Catalyzed Dehydrogenative Cross-Coupling Reaction. *Adv. Synth. Catal.* **2013**, *355*, 1971–1976. [CrossRef]
77. Huang, C.; Wang, J.-H.; Qiao, J.; Fan, X.-W.; Chen, B.; Tung, C.-H.; Wu, L.-Z. Direct Arylation of Unactivated Alkanes with Heteroarenes by Visible-Light Catalysis. *J. Org. Chem.* **2019**, *84*, 12904–12912. [CrossRef] [PubMed]
78. Quattrini, M.C.; Fujii, S.; Yamada, K.; Fukuyama, T.; Ravelli, D.; Fagnoni, M.; Ryu, I. Versatile Cross-Dehydrogenative Coupling of Heteroaromatics and Hydrogen Donors via Decatungstate Photocatalysis. *Chem. Commun.* **2017**, *53*, 2335–2338. [CrossRef] [PubMed]
79. Bhakat, M.; Khatua, B.; Guin, J. Photocatalytic Aerobic Coupling of Azaarenes and Alkanes via Nontraditional Cl $^{\bullet}$ Generation. *Org. Lett.* **2022**, *24*, 5276–5280. [CrossRef]
80. Jung, S.; Lee, H.; Moon, Y.; Jung, H.-Y.; Hong, S. Site-Selective C–H Acylation of Pyridinium Derivatives by Photoredox Catalysis. *ACS Catal.* **2019**, *9*, 9891–9896. [CrossRef]
81. Tian, H.; Yang, H.; Tian, C.; An, G.; Li, G. Cross-Dehydrogenative Coupling of Strong C(Sp^3)–H with *N* -Heteroarenes through Visible-Light-Induced Energy Transfer. *Org. Lett.* **2020**, *22*, 7709–7715. [CrossRef] [PubMed]
82. Huang, C.-Y.; Li, J.; Liu, W.; Li, C.-J. Diacetyl as a "Traceless" Visible Light Photosensitizer in Metal-Free Cross-Dehydrogenative Coupling Reactions. *Chem. Sci.* **2019**, *10*, 5018–5024. [CrossRef]
83. Li, L.; Song, X.; Qi, M.-F.; Sun, B. Weak Brønsted Base-Promoted Photoredox Catalysis for C-H Alkylation of Heteroarenes Mediated by Triplet Excited Diaryl Ketone. *Tetrahedron Lett.* **2022**, *99*, 153846. [CrossRef]
84. Bhakat, M.; Biswas, P.; Dey, J.; Guin, J. Heteroarylation of Ethers, Amides, and Alcohols with Light and O_2. *Org. Lett.* **2021**, *23*, 6886–6890. [CrossRef]
85. Zhao, H.; Li, Z.; Jin, J. Green Oxidant H_2O_2 as a Hydrogen Atom Transfer Reagent for Visible Light-Mediated Minisci Reaction. *New J. Chem.* **2019**, *43*, 12533–12537. [CrossRef]
86. Zhang, L.; Zhang, G.; Li, Y.; Wang, S.; Lei, A. The Synergistic Effect of Self-Assembly and Visible-Light Induced the Oxidative C–H Acylation of N-Heterocyclic Aromatic Compounds with Aldehydes. *Chem. Commun.* **2018**, *54*, 5744–5747. [CrossRef] [PubMed]
87. Li, X.; Liu, C.; Guo, S.; Wang, W.; Zhang, Y. PIFA-Mediated Cross-Dehydrogenative Coupling of *N* -Heteroarenes with Cyclic Ethers: Ethanol as an Efficient Promoter. *Eur. J. Org. Chem.* **2021**, *2021*, 411–421. [CrossRef]
88. Utepova, I.A.; Trestsova, M.A.; Chupakhin, O.N.; Charushin, V.N.; Rempel, A.A. Aerobic Oxidative C–H/C–H Coupling of Azaaromatics with Indoles and Pyrroles in the Presence of TiO_2 as a Photocatalyst. *Green Chem.* **2015**, *17*, 4401–4410. [CrossRef]
89. Li, Z.; Wu, L.; Guo, J.; Shao, Y.; Song, Y.; Ding, Y.; Zhu, L.; Yao, X. Light-Promoted Minisci Coupling Reaction of Ethers and Aza Aromatics Catalyzed by Au/TiO_2 Heterogeneous Photocatalyst. *ChemCatChem* **2021**, *13*, 3671–3678. [CrossRef]
90. Qiao, J.; Song, Z.; Huang, C.; Ci, R.; Liu, Z.; Chen, B.; Tung, C.; Wu, L. Direct, Site-Selective and Redox-Neutral A-C−H Bond Functionalization of Tetrahydrofurans via Quantum Dots Photocatalysis. *Angew. Chem. Int. Ed.* **2021**, *60*, 27201–27205. [CrossRef] [PubMed]
91. Vijeta, A.; Reisner, E. Carbon Nitride as a Heterogeneous Visible-Light Photocatalyst for the Minisci Reaction and Coupling to H_2 Production. *Chem. Commun.* **2019**, *55*, 14007–14010. [CrossRef] [PubMed]
92. Boyd, A.A.; Flaud, P.-M.; Daugey, N.; Lesclaux, R. Rate Constants for RO_2 + HO_2 Reactions Measured under a Large Excess of HO_2. *J. Phys. Chem. A* **2003**, *107*, 818–821. [CrossRef]
93. Opeida, I.A.; Sheparovych, R.B. Inhibition by Hydrogen Peroxide in the Radical Chain Oxidation of Hydrocarbons by Molecular Oxygen. *Theor. Exp. Chem.* **2019**, *55*, 36–42. [CrossRef]
94. Opeida, I.A.; Sheparovych, R.B.; Hrynda, Y.M.; Khavunko, O.Y.; Kompanets, M.O.; Shendryk, A.N. Kinetics of Oxidation of Benzyl Alcohols with Molecular Oxygen Catalyzed by *N*-hydroxyphthalimide: Role of Hydroperoxyl Radicals. *Int. J. Chem. Kinet.* **2019**, *51*, 679–688. [CrossRef]
95. Patil, S.V.; Tanko, J.M. Radical Additions of Acyclic and Cyclic Ethers to Alkenes via an Allyl Transfer Reaction Involving Phthalimido-N-Oxyl Radical. *Tetrahedron* **2016**, *72*, 7849–7858. [CrossRef]
96. Terent'ev, A.O.; Platonov, M.M.; Krylov, I.B.; Chernyshev, V.V.; Nikishin, G.I. Synthesis of 1-Hydroperoxy-1′-Alkoxyperoxides by the Iodine-Catalyzed Reactions of Geminal Bishydroperoxides with Acetals or Enol Ethers. *Org. Biomol. Chem.* **2008**, *6*, 4435. [CrossRef] [PubMed]
97. Terent'ev, A.O.; Sharipov, M.Y.; Krylov, I.B.; Gaidarenko, D.V.; Nikishin, G.I. Manganese Triacetate as an Efficient Catalyst for Bisperoxidation of Styrenes. *Org. Biomol. Chem.* **2015**, *13*, 1439–1445. [CrossRef] [PubMed]
98. Terent'ev, A.; Borisov, D.; Semenov, V.; Chernyshev, V.; Dembitsky, V.; Nikishin, G. Selective Synthesis of Unsymmetrical Peroxides: Transition-Metal-Catalyzed Oxidation of Malononitrile and Cyanoacetic Ester Derivatives by Tert-Butyl Hydroperoxide at the α-Position. *Synthesis* **2011**, *2011*, 2091–2100. [CrossRef]
99. Pastori, N.; Gambarotti, C.; Punta, C. Recent Developments in Nucleophilic Radical Addition to Imines: The Key Role of Transition Metals and the New Porta Radical-Type Version of the Mannich and Strecker Reactions. *MROC* **2009**, *6*, 184–195. [CrossRef]
100. Vil', V.A.; Grishin, S.S.; Baberkina, E.P.; Kostyagina, V.A.; Kovalenko, A.E.; Terent'ev, A.O. Radical Addition of Tetrahydrofuran to Imines Assisted by Tert-Butyl Hydroperoxide. *Tetrahedron Lett.* **2020**, *61*, 152150. [CrossRef]

101. Clerici, A.; Cannella, R.; Pastori, N.; Panzeri, W.; Porta, O. A Free Radical Mannich Type Reaction: Selective α-CH Aminomethylation of Ethers by Ti(III)/t-BuOOH System under Aqueous Acidic Conditions. *Tetrahedron* **2006**, *62*, 5986–5994. [CrossRef]
102. Zhang, Y.; Zhang, S.; Xu, G.; Li, M.; Tang, C.; Fan, W. Cu-Catalyzed Carbamoylation *versus* Amination of Quinoline *N*-Oxide with Formamides. *Org. Biomol. Chem.* **2019**, *17*, 309–314. [CrossRef] [PubMed]
103. Godugu, K.; Nallagondu, C.G.R. Solvent and Catalyst-free Synthesis of Imidazo[1,2-a]Pyridines by Grindstone Chemistry. *J. Heterocycl. Chem.* **2021**, *58*, 250–259. [CrossRef]
104. Wen, J.; Li, X.; Li, H.; Ma, S.; He, K.; Xu, Y.; Fang, Y.; Liu, W.; Gao, Q. Enhanced Visible-Light H_2 Evolution of g-C_3N_4 Photocatalysts via the Synergetic Effect of Amorphous NiS and Cheap Metal-Free Carbon Black Nanoparticles as Co-Catalysts. *Appl. Surf. Sci.* **2015**, *358*, 204–212. [CrossRef]
105. Yao, S.; Xue, S.; Peng, S.; Jing, M.; Qian, X.; Shen, X.; Li, T.; Wang, Y. Synthesis of Graphitic Carbon Nitride at Different Thermal-Pyrolysis Temperature of Urea and It Application in Lithium–Sulfur Batteries. *J. Mater. Sci. Mater. Electron.* **2018**, *29*, 17921–17930. [CrossRef]
106. Sankari Devi, E.; Alanthadka, A.; Tamilselvi, A.; Nagarajan, S.; Sridharan, V.; Maheswari, C.U. Metal-Free Oxidative Amidation of Aldehydes with Aminopyridines Employing Aqueous Hydrogen Peroxide. *Org. Biomol. Chem.* **2016**, *14*, 8228–8231. [CrossRef]